SUPPLEMENTARY INFORMATION

Noise and Low-Level Dynamics Can Coordinate Multicomponent Bet Hedging Mechanisms

Javier Garcia-Bernardo[1], *Mary J. Dunlop*[2,*]
[1] *Department of Computer Science, University of Vermont, Burlington, VT, USA 05405*
[2] *School of Engineering, University of Vermont, Burlington, VT, USA 05405*
[*] *mjdunlop@uvm.edu*

SUPPLEMENTARY FIGURES

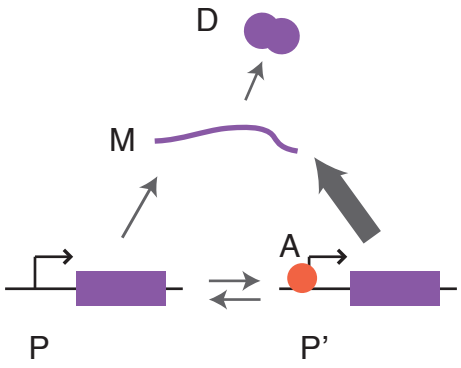

Figure S1. Schematic of the chemical reactions in the model. A, activator; P, unbound promoter; P', bound promoter; M, mRNA; D, downstream gene. Reactions and their rates are listed in Table S1.

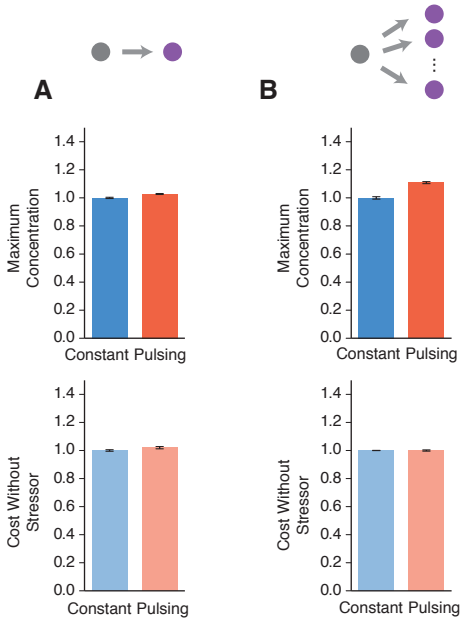

Figure S2. Linear cost function. The maximum concentration of stressor that 0.1% of cells in a population can survive and the corresponding average cost of growing in the absence of stressor. Values were measured for constant and pulsing activator dynamics for (A) one downstream gene and (B) ten downstream genes with K_D = 10,000 molecules. The cost function is linear (Methods). Error bars show standard deviations over three simulations.

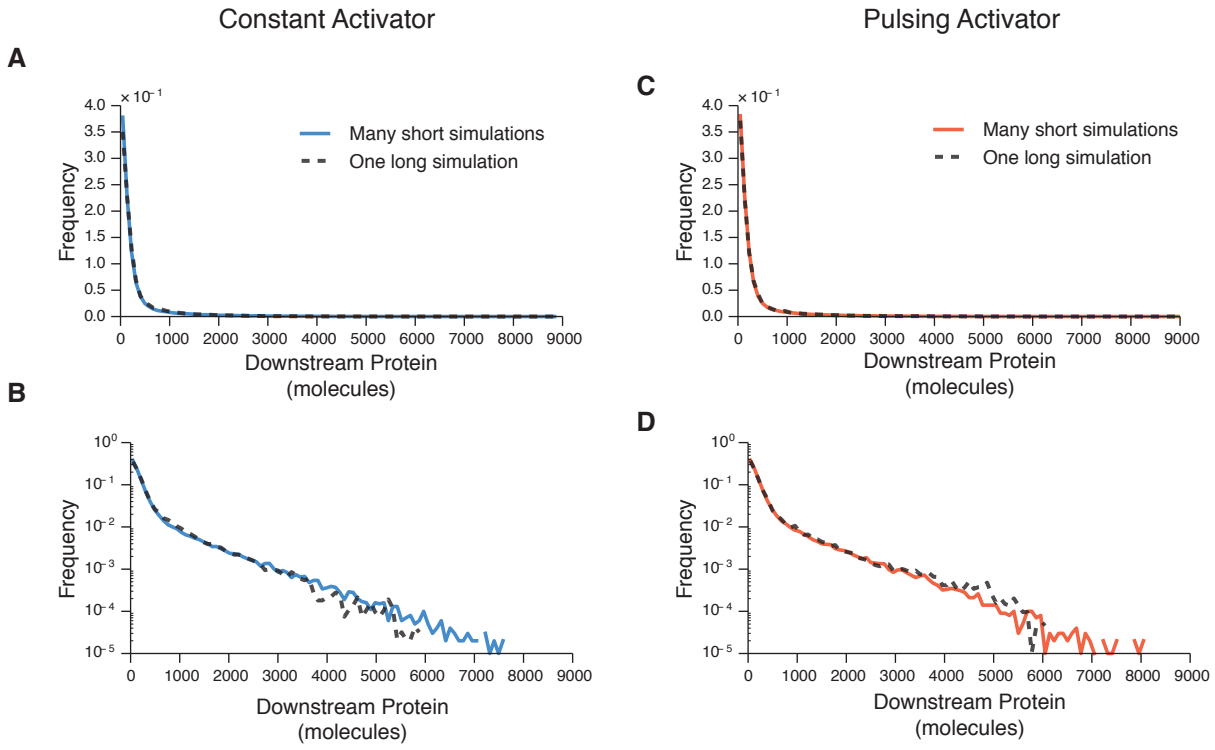

Figure S3. Histogram of downstream protein levels are equivalent when comparing data generated using a single 10^5 minute simulation (dashed line) and the final data points from 10^5 independent simulations (solid line). (A-B) Constant input distributions of downstream proteins plotted on (A) linear and (B) log scales. (C-D) Pulsing input distributions on (C) linear and (D) log scales.

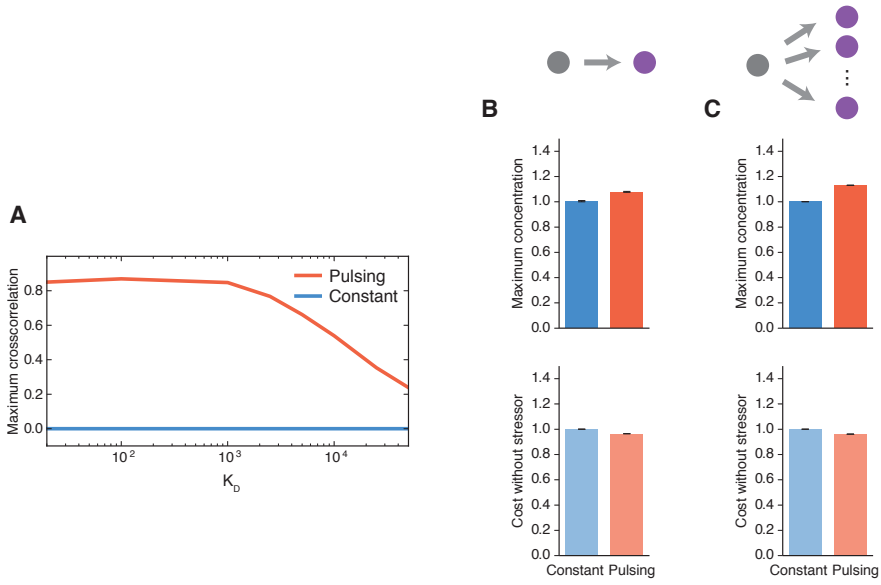

Figure S4. Fast promoter dynamics. (A) Maximum cross correlation as a function of the dissociation constant, K_D. (B, C) Maximum survivable concentration of stressor and the corresponding average cost of growing in the absence of stressor for constant and pulsing activator dynamics with (B) one downstream gene and (C) ten downstream genes with K_D = 10,000 molecules. Values from the pulsing dynamics are normalized to the constant input case. Error bars show standard deviations over three simulations.

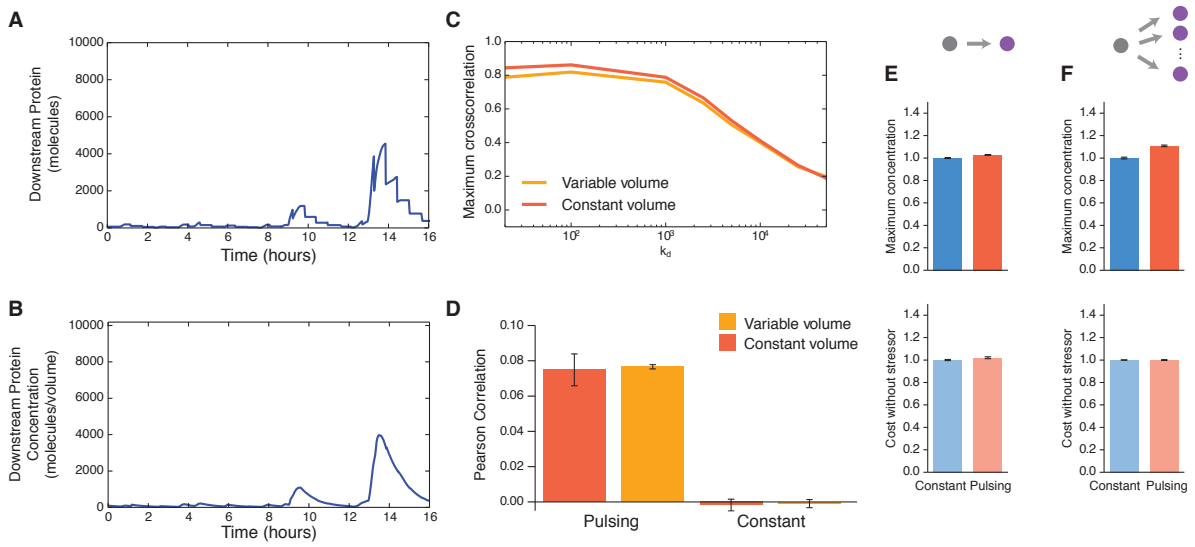

Figure S5. Effect of growth and partitioning on coordination. (A) Simulation with cell growth and partitioning showing the number of molecules of a downstream genes controlled by a pulsing input; K_D = 10,000 molecules. (B) Concentration of the downstream protein. In this plot the data from (A) is divided by the cell volume, which changes with time. (C) Maximum cross correlation between a pulsing activator and downstream protein as a function of K_D. The data generated using the model with cell division is similar to that without division and growth modeled explicitly, especially for large K_D values. (D) Pearson correlation between two downstream genes with K_D = 10,000 under the control of a pulsing input with and without growth and partitioning. (E, F) The maximum concentration of stressor that 0.1% of cells in a population can survive and the corresponding average cost of growing in the absence of stressor, when the effect of growth and partitioning are included. Values were measured for constant and pulsing activator dynamics for (E) one downstream gene and (F) ten downstream genes with K_D = 10,000 molecules. Error bars show standard deviations over three simulations.

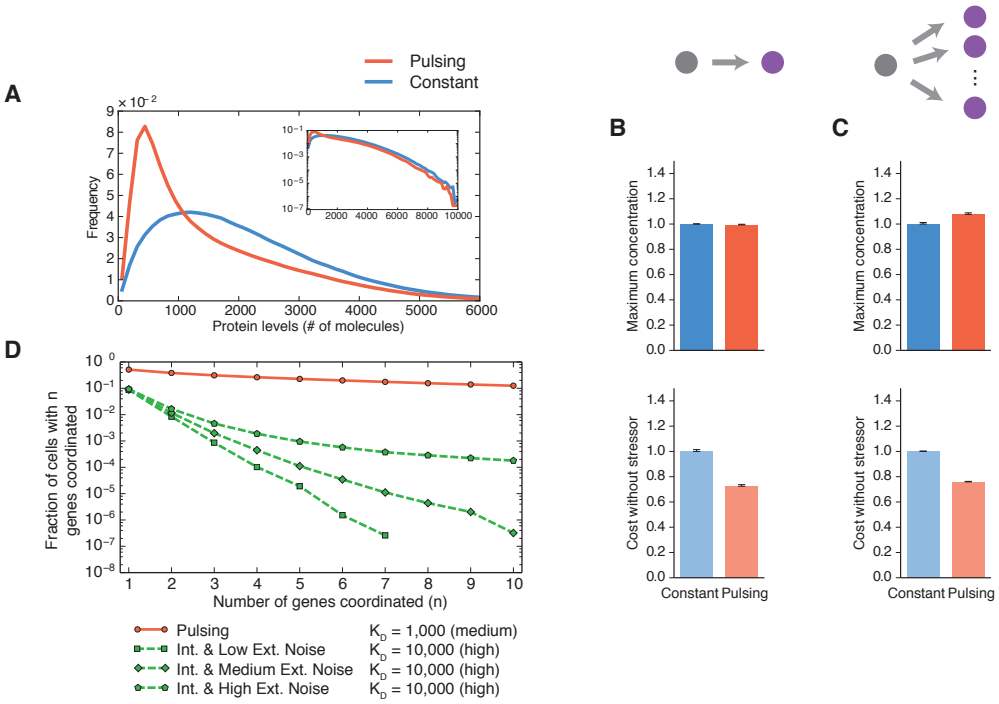

Figure S6. Medium dissociation constant (K_D = 1000 molecules). (A) Histograms of downstream gene expression. Inset shows the same data on a semilogarithmic scale. Note that the distributions are not identical due to the nonlinear nature of the activator curve: the pulsatile input spends more time at low values on the activation curve than the constant input does, resulting in lower mean expression of the downstream gene. (B, C) Maximum survivable concentration of stressor and the corresponding average cost of growing in the absence of stressor for constant and pulsing activator dynamics with (B) one downstream gene and (C) ten downstream genes with K_D = 1000 molecules. Values from the pulsing dynamics are normalized to the constant input case. Error bars show standard deviations over three simulations. (D) The fraction of cells with all downstream genes coordinated as a function of the number of downstream genes, *n*. The three noise data cases are reproduced from Fig. 4 for context and show results for infrequently activated downstream genes (K_D = 10,000 molecules). The pulsing data is for downstream genes with a medium dissociation constant (K_D = 1000 molecules). The plots do not start at the same point when *n* = 1 because the probability that a medium K_D gene is above the threshold for survival is greater than the probability that a high K_D gene is above the same threshold.

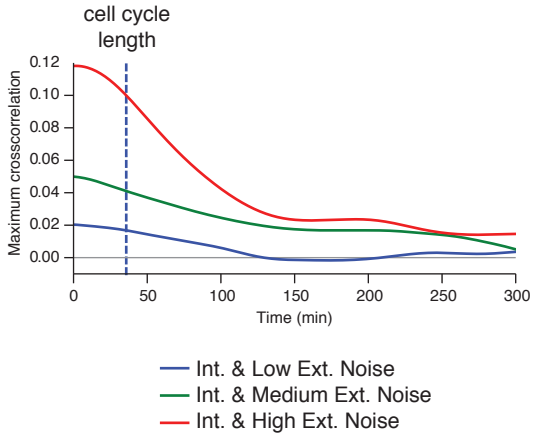

Figure S7. Cross correlation between two downstream genes (K_D = 10,000 molecules) with a noisy activator input. The three noise levels correspond to those shown in Fig. 3E and F.

SUPPLEMENTARY TEXT

Probability of coordination from dynamic and constant inputs

To gain further insight into the effects of coordination, we calculated the probabilities of coordinating *n* downstream genes using a simplified system, comparing a constant input with a simple dynamic input modeled by a square wave signal.

$$A_{constant} = X$$

$$A_{dynamic} \begin{cases} X\frac{T_{ON} + T_{OFF}}{T_{ON}}, & 0 < t \leq T_{ON} \\ 0, & T_{ON} < t \leq T_{OFF} \end{cases}$$

Note that, by construction, the two signals have the same mean. We assumed that the probability of turning on expression of a downstream gene is linearly related to the input, such that higher inputs result in an increased probability of activating the downstream gene. We found this to be a reasonable assumption based on empirical fits to our data (Supplementary Methods). The probability of coordinating *n* genes is the probability that all downstream genes are coordinated simultaneously

$$p(n) = (\gamma A)^n$$

Comparing the two types of inputs, we find

$$p_{constant}(n) = (\gamma X)^n$$

$$p_{dynamic}(n) = \frac{T_{ON}}{T_{ON} + T_{OFF}}(\gamma X \frac{T_{ON} + T_{OFF}}{T_{ON}})^n + \frac{T_{OFF}}{T_{ON} + T_{OFF}}(\gamma X\ 0)^n$$

$$= \left(\frac{T_{ON} + T_{OFF}}{T_{ON}}\right)^{n-1} (\gamma X)^n$$

The ratio of the two probabilities is

$$\frac{p_{dynamic}(n)}{p_{constant}(n)} = \left(\frac{T_{ON} + T_{OFF}}{T_{ON}}\right)^{n-1}$$

Therefore, the probability of coordinating *n* genes is always higher with pulsing than with a constant inputs when $n > 1$

$$p_{dynamic}(n) > p_{constant}(n)$$

Note that the two probabilities are equal when $n = 1$, as expected since coordination requires more than one gene.

SUPPLEMENTARY METHODS

Fast dynamics and moderate affinity downstream gene

Fast dynamics (Fig. S4) were modeled by increasing K_{ON} and K_{OFF}, as listed in Table S1, by a factor of 10. Note that the dissociation constant K_D ($=K_{OFF}/K_{ON}$) stays the same.

For the moderate affinity downstream gene (Fig. S6) K_D = 1000 molecules.

Coordination of *n* downstream genes

In the probability calculations described above we assumed a linear relationship between the probability of turning on expression of a downstream gene and the concentration of the activator. We determined the linear relationship empirically, finding $\gamma = 3.85 \times 10^{-4}$, by using Eureqa (1). This relationship holds for the thresholds described above with $R^2 > 0.99$ for the linear regression fit.

Modeling growth and partitioning

We assumed a cell division time of 34.7 minutes (equal to –ln(2)/0.02, the protein degradation half-life from Table S1). During growth, cellular volume increased following $V(t) = V_0 \, 2^{t/34.7}$, where t is the time from the previous cell division event and V_0 was set to ln(2) to allow for a mean volume of 1. At every cell division event, cellular volume was reset to V_0 and the contents of the cell, including all protein, mRNA, and DNA species were partitioned between two daughter cells following a negative binomial distribution with probability 0.5. This distribution measures the number of molecules that are partitioned between each cell, assuming that every molecule is independent and has equal probability of being transmitted to each daughter cell. With variable volume, the units of K_{OFF} (Table S1) become V_r/min^{-1}, where V_r is the normalized volume, or volume/average volume. The pulsing signal was adjusted to match the dynamics of the case with fixed volume. To achieve this, at every time step the number of molecules of the activator was divided by the normalized volume. However, instead of multiplying K_{OFF} by V_r and dividing the number of molecules by V_r, K_{OFF} was held constant during the simulation and the number of molecules of the activator was varied according to the pulsing signal, and not corrected by volume.

Equivalence of long time simulation and many short time simulations

We verified that distributions of downstream protein levels generated using long simulations are equivalent to those generated by running many shorter simulations. This approach reduces the computation time required to generate data. For the long time course simulations in Fig. S3, we first performed an initialization simulation of 1440 minutes (24 hours) and used the final values from these data to set initial conditions. We then ran 10^5 minute simulations. For the short time simulations (Fig. S3), we used the initialization step and ran 10^5 simulations of 1440 minutes each, where the input activator signal had a random phase drawn from a uniform distribution between 0 and 240 minutes (corresponding to the period of the signal) to avoid sampling at the same point in the cycle every time.

Table S1. Reaction rates

Reaction rate	Value	Reaction	Comments

K_D	10,000 molecules		We set the amplitude of the pulses one order of magnitude lower than the K_D. One order of magnitude between the K_D of regulated genes has been observed experimentally (2, 3).
K_{OFF}	0.1 min^{-1}	$P' \rightarrow P + A$	Selected based on studies from both yeast and bacteria (3-5).
K_{ON}	K_{OFF}/K_D (molecules $min)^{-1}$	$P + A \rightarrow P'$	
α	0.02 min^{-1}	$P \rightarrow P + M$	Basal expression
α’	2 min^{-1}	$P' \rightarrow P' + M$	One order of magnitude higher than typical transcription rates in both in yeast (6) and *E. coli* (7). Note that these rates are based on only one RNA polymerase molecule, and several molecules work at the same time, therefore we increased the rate by an order of magnitude. The results are not sensitive to the exact value of α’.
λ_M	0.1 min^{-1}	$M \rightarrow \emptyset$	Typical degradation rate in *E. coli* (8) and in the feasible range for yeast (9).
β	10 min^{-1}		One order of magnitude higher than typical translation rates in *E. coli* (10), yeast (11), and mice (12). Note that these results are based on only one ribosome complex per mRNA, and several can work at the same time; the typical lag between translation initiation is 15 seconds in *E. coli* (13). The results are not sensitive to the exact value of β.
λ_D	0.02 min^{-1}		We used a typical half-life of 34.7 min, which corresponds with a stable protein in *E. coli* or a moderately degraded protein in yeast (14, 15).

Table S2. K_{ON} and noise contributions for different activator profiles. The K_{ON} value from Table S1 is multiplied by the constants listed here. $\eta_{tot}^2 = \eta_{int}^2 + \eta_{ext}^2$

Activator profile	**K_{ON} scaling factor**	**Total Noise (η_{tot})**	**Intrinsic Noise (η_{int})**	**Extrinsic Noise (η_{ext})**
Constant expression	1	0	0	0
Only Intrinsic Noise	1	0.21	0.21	0
Intrinsic & Low Extrinsic Noise	1.052	0.24	0.21	0.11

Intrinsic & Medium Extrinsic Noise	1.266	0.29	0.21	0.20
Intrinsic & High Extrinsic Noise	1.626	0.34	0.21	0.27

REFERENCES

1. Schmidt, M., and H. Lipson. 2013. Eureqa (Version 0.98 beta) [Software]. Available from http://www.eureqa.com/.
2. Lee, P., B.-R. Cho, H.-S. Joo, and J.-S. Hahn. 2008. Yeast Yak1 kinase, a bridge between PKA and stress-responsive transcription factors, Hsf1 and Msn2/Msn4. Molecular microbiology 70:882-895.
3. Hansen, A. S., and E. K. O'Shea. 2013. Promoter decoding of transcription factor dynamics involves a trade-off between noise and control of gene expression. Molecular systems biology 9:704.
4. So, L.-H., A. Ghosh, C. Zong, L. a. Sepúlveda, R. Segev, and I. Golding. 2011. General properties of transcriptional time series in Escherichia coli. Nature genetics 43:554-560.
5. China, A., P. Tare, and V. Nagaraja. 2010. Comparison of promoter-specific events during transcription initiation in mycobacteria. Microbiology (Reading, England) 156:1942-1952.
6. Pelechano, V., S. Chávez, and J. Pérez-Ortín. 2010. A complete set of nascent transcription rates for yeast genes. PLoS One 5.
7. Davenport, R. J., G. J. L. Wuite, R. Landick, and C. Bustamante. 2000. Single-Molecule Study of Transcriptional Pausing and Arrest by. Science 287:2497-2500.
8. Selinger, D. W., R. M. Saxena, K. J. Cheung, G. M. Church, and C. Rosenow. 2003. Global RNA Half-Life Analysis in Escherichia coli Reveals Positional Patterns of Transcript Degradation. Genome research 13:216-223.
9. Wang, Y., C. L. Liu, J. D. Storey, R. J. Tibshirani, D. Herschlag, and P. O. Brown. 2002. Precision and functional specificity in mRNA decay. Proceedings of the National Academy of Sciences of the United States of America 99:5860-5865.
10. Sørensen, M., C. Kurland, and S. Pedersen. 1989. Codon usage determines translation rate in Escherichia coli. Journal of molecular biology 207:365-377.
11. Bonven, B., and K. Gulløv. 1979. Peptide chain elongation rate and ribosomal activity in Saccharomyces cerevisiae as a function of the growth rate. Molecular and General Genetics 170:225-230.
12. Schwanhäusser, B., D. Busse, N. Li, G. Dittmar, J. Schuchhardt, J. Wolf, W. Chen, and M. Selbach. 2011. Global quantification of mammalian gene expression control. Nature 473:337-342.
13. Siwiak, M., and P. Zielenkiewicz. 2013. Transimulation - protein biosynthesis web service. PLoS One 8:e73943.
14. Belle, A., A. Tanay, L. Bitincka, R. Shamir, and E. K. O'Shea. 2006. Quantification of protein half-lives in the budding yeast proteome. Proceedings of the National Academy of Sciences of the United States of America 103:13004-13009.
15. Woldringh, C. L., M. a. de Jong, W. van den Berg, and L. Koppes. 1977. Morphological analysis of the division cycle of two Escherichia coli substrains during slow growth. Journal of bacteriology 131:270-279.